# Possible origin of memory in earthquakes: Real catalogs and an epidemic-type aftershock sequence model

Jingfang Fan,[1,2,3,*] Dong Zhou,[1,2,4,5] Louis M. Shekhtman,[2,†] Avi Shapira,[6] Rami Hofstetter,[7] Warner Marzocchi,[8] Yosef Ashkenazy,[1] and Shlomo Havlin[2]

[1]*Blaustein Institutes for Desert Research, Ben-Gurion University of the Negev, Midreshet Ben-Gurion 84990, Israel*

[2]*Department of Physics, Bar Ilan University, Ramat Gan 52900, Israel*

[3]*Potsdam Institute for Climate Impact Research, 14412 Potsdam, Germany*

[4]*School of Reliability and Systems Engineering, Beihang University, Beijing, 100191, China*

[5]*Science and Technology on Reliability and Environmental Engineering Laboratory, 100191 Beijing, China*

[6]*National Institute for Regulation of Emergency and Disaster, College of Law and Business, Bnei Brak, 511080, Israel*

[7]*Geophysical Institute of Israel, Lod 7019802, Israel*

[8]*Department of Earth, Environmental, and Resources Sciences, University of Naples, Federico II, Complesso di Monte Sant'Angelo, Via Cinthia, 21 80126 Napoli, Italy*

(Received 27 July 2018; revised manuscript received 4 April 2019; published 19 April 2019)

Earthquakes are one of the most devastating natural disasters that plague society. Skilled, reliable earthquake forecasting remains the ultimate goal for seismologists. Using the detrended fluctuation analysis (DFA) and conditional probability (CP) methods, we find that memory exists not only in interoccurrence seismic records but also in released energy as well as in the series of the number of events per unit time. Analysis of a standard epidemic-type aftershock sequences (ETAS) earthquake model indicates that the empirically observed earthquake memory can be reproduced only for a narrow range of the model's parameters. This finding therefore provides tight constraints on the model's parameters and can serve as a testbed for existing earthquake forecasting models. Furthermore, we show that by implementing DFA and CP results, the ETAS model can significantly improve the short-term forecasting rate for the real (Italian) earthquake catalog.

DOI: 10.1103/PhysRevE.99.042210

## I. INTRODUCTION

The process through which earthquakes occur is complex, involving spatiotemporal dynamics [1,2], and has previously been characterized as a paradigm of self-organized criticality [3,4]. However, the underlying mechanisms of earthquakes are still not fully understood [5], and as a consequence, forecasting event magnitude, location, and time in advance remains elusive. Over the past decades, scaling laws for the distribution of waiting times between earthquake events have been obtained for seismic data [3,6] and for rock fracture [7], as well as for "Woodquakes" [8] laboratory experiments. Perhaps the most promising observation is that a rescaling involving region size and magnitude threshold produces data collapse onto a universal $\gamma$ distribution for many worldwide regions [6]. This observation is of great importance for the development of physical and statistical models of earthquake dynamics. However, an analysis on the ETAS model has indicated that this distribution is not universal [9,10] but instead is a bimodal mixture distribution [11]. These modeling studies have captured much of the earthquake dynamics through the distribution of recurrence intervals, but they have not considered the memory found in real earthquake time series. Ribeiro *et al.* reported the analogies between the cracking noise of ethanol-dampened charcoal and earthquakes and found that the most fundamental seismic laws are valid in their experiments [12].

Long-term memory has been reported in many natural systems, such as the climate system [13–15], physiology [16,17], and in seismic activity [18,19]. For example, Livina *et al.* found that consecutive recurrence times (for different magnitude threshold) depend on each other, such that both short and long recurrence times tend to cluster in time (i.e., short interevent after short interevent and long interevent after long interevent) [18]. Later, Lennartz *et al.* [19] studied the Northern and Southern California earthquake catalogs and found long-term memory using the detrended fluctuation analysis (DFA). The goal of the present study is to uncover the mechanisms that underlie the memory observed in earthquake data.

The structure of our paper is as follows: In the next section, we describe and introduce DFA for the real seismic catalogs. In Sec. III, conditional probability analysis for the real seismic catalogs is presented. In Sec. IV we discuss the memory analysis in the ETAS model. In Sec. V results of earthquake forecasting are shown. Finally, in Sec. VI a short summary and outlook are provided.

## II. DETRENDED FLUCTUATION ANALYSIS FOR THE REAL SEISMIC CATALOGS

DFA [20] is often used to detect long-range correlations of diverse time series, including DNA sequences [21], heart rate [16,17,22], and climate records [15]. When the time series is

*jingfang@pik-potsdam.de
†lsheks@gmail.com

 

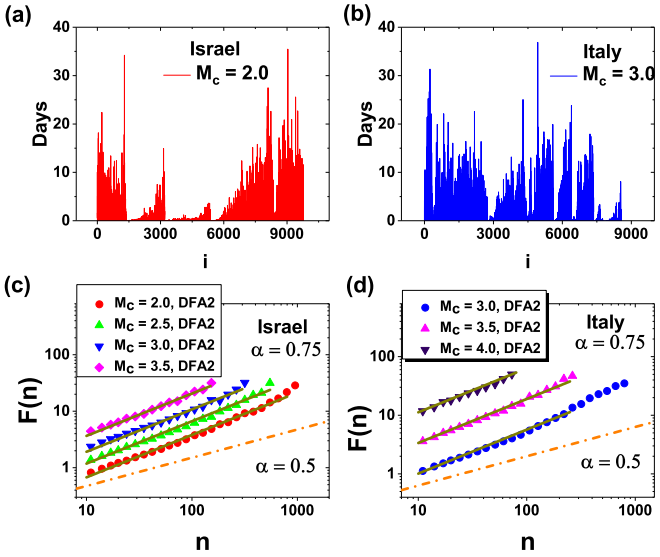


FIG. 1. Interoccurrence time series between earthquake events from the Israeli (a) and Italian (b) catalogs using magnitude threshold $M_c$. DFA of the interoccurrence times from the (c) Israeli and (d) Italian catalogs with different $M_c$ values. The solid lines are the best fit lines with slope $\alpha \approx 0.75$; the R-squared is larger than 0.99. For comparison we also include a dashed-dotted line that indicates no memory ($\alpha = 0.5$).

long-range correlated, the fluctuation function$F(n)$ increases according to a power-law relation: $F(n) \sim n^{\alpha}$ where $n$ is the window size and $\alpha$ is the scaling exponent. Here, $F(n) = \sqrt{\frac{1}{n}\sum_{t=1}^{n}(X_t - Y_t)^2}$, where $X_t = \sum_{i=1}^{t}(x_i - \langle x \rangle)$ is the cumulative sum or the "profile" of a time series $x_i$, and $Y_t$ is the fitting polynomial. The exponent $\alpha$ is calculated as the slope of a linear fit to the log-log graph of $F(n)$ vs $n$. An exponent $\alpha = 0.5$ indicates the absence of correlations (white noise), whereas $\alpha > 0.5$ indicates long-range correlations in the time series where higher values of $\alpha$ imply stronger correlations.

Here we study the long-term memory in the real seismic catalogs of Italy and Israel [23,24]. Figure 1 shows the results on examples of the return intervals (days) in the Israeli (from 1981 to 2017) and Italian (from 1986 to 2017) seismic catalogs using different magnitude thresholds $M_c$. Note that the earthquake events with $M \geqslant 2.0$ (3.0) for Israeli (Italian) are complete, meaning that all earthquakes above this magnitude are included in the catalog. The DFA results of the return intervals time series indicate the existence of similar long-term memory in both the Israeli and Italian earthquake catalogs [Figs. 1(c) and 1(d)]. The estimated scaling exponent is $\alpha \sim 0.75$ and is independent of the magnitude $M_c$ [see also Figs. 2(a) and 2(b)]; this value is consistent with a previous study of the Southern and Northern California catalogs [19].

To validate the existence of the long correlations, we also analyzed the randomly reshuffled earthquake catalog records. The shuffling procedure destroys the correlations between the return intervals but keeps the distribution of the return intervals unaffected. We calculated the averaged $\alpha\pm$ the standard deviation of 1000 such shuffled records [Figs. 2(a) and 2(b)] and found that the exponents of the real data are significantly larger than the exponents of the shuffled data, validating the

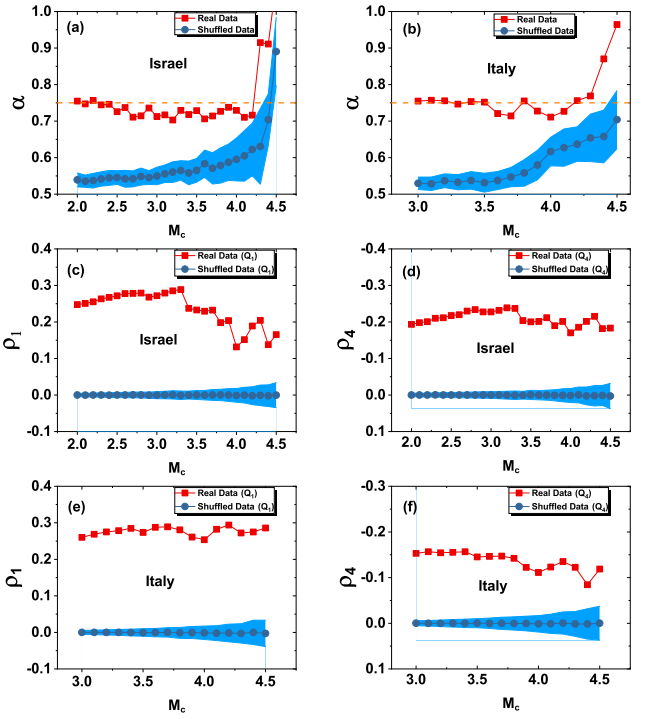


FIG. 2. DFA scaling exponent $\alpha$ as a function of the magnitude threshold $M_c$ for the (a) Israeli and (b) Italian catalogs. CP memory coefficients $\rho_1$ and $\rho_4$ are shown as a function of magnitude threshold $M_c$ for the (c, d) Israeli and (e, f) Italian catalogs. The blue line (circles) in the bottom of each subplot depicts the mean results of randomly shuffled records, averaged over 1000 realizations; the shaded area indicates the error bars (std.).

existence of long-range correlations in the real data. The large increase in the scaling exponent in both real and shuffled data for large $M_c$ is probably due to finite size effects [25].

We also performed DFA on other seismic variables, such as the number of earthquake events and the released energy

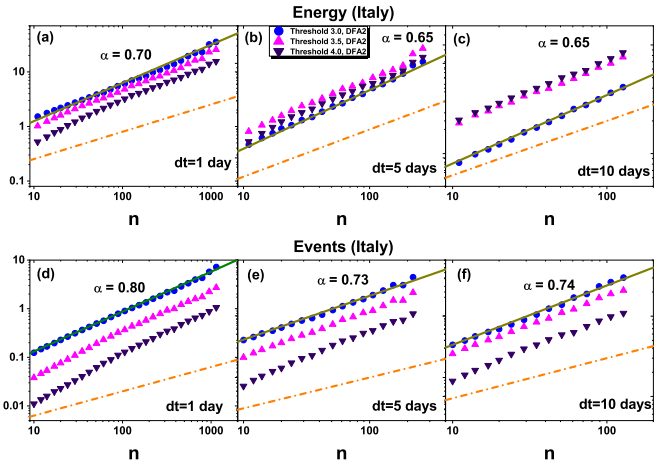


FIG. 3. DFA of (a, b, c) the released energy time series and (d, e, f) the number of events time series within a $dt$ time period for the Israeli catalog. The solid lines are the best fitting lines with slope $\alpha$ where R-squared $> 0.99$. For comparison, the dashed-dotted line with slope $\alpha = 0.5$, indicating no memory, is presented.

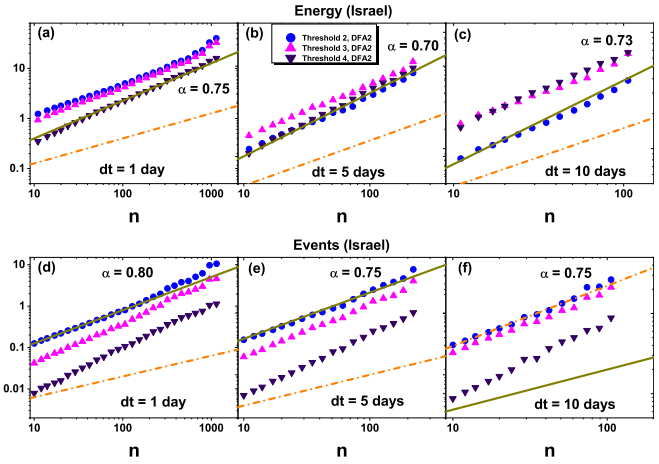


FIG. 4. DFA of (a, b, c) the released energy time series and (d, e, f) the number of events time series within a $dt$ time period for the Italian catalog. The solid lines are the best fitting lines with slope $\alpha$ where R-squared $> 0.99$. For comparison, the dashed-dotted line with slope $\alpha = 0.5$, indicating no memory, is presented.

within a coarse time window $dt$. To analyze the energy associated with the earthquakes, for each catalog we define a time series [26], $S(t) = \sum_{l=1}^{E(t)} 10^{\frac{3}{2}M_l(t)}$, where $E(t)$ denotes the number of events that occurred between $t$ and $t + dt$, and $M_l(t)$ denotes the magnitude of the event. The time series is proportional to the total energy released in a $dt$ time period. To deal with more homogeneous time series we switch to $s(t) = \log(S(t))$ for $S(t) > 1$ and zero for $S(t) \leqslant 1$, and $e(t) = \log(E(t))$ for $E(t) > 1$ and zero for $E(t) \leqslant 1$. This (log) operation aims to suppress extremely high values of $E(t)$ and $S(t)$ that can affect $F(n)$ and its correlation exponent $\alpha$. Figures 3 and 4 depict the DFA analysis for the earthquake magnitude time series $s(t)$ and for the number of events time series $e(t)$ for the Israeli and Italian catalogs for different time windows $dt$. We find that for both countries and for all studied magnitudes the value of the scaling exponent $\alpha$ is quite

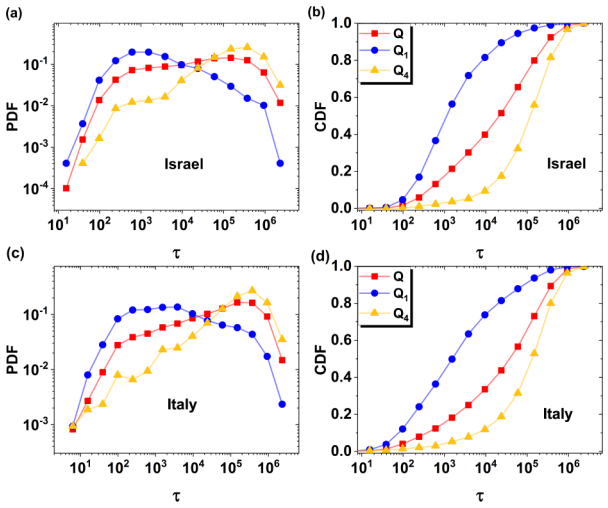


FIG. 5. (a, c) Conditional PDF and (b, d) CDF of the recurrence times $\tau$ for the (a, b) Israeli catalog above the threshold $M_c = 2.0$ and for the (c, d) Italian catalog above the threshold $M_c = 3.0$.

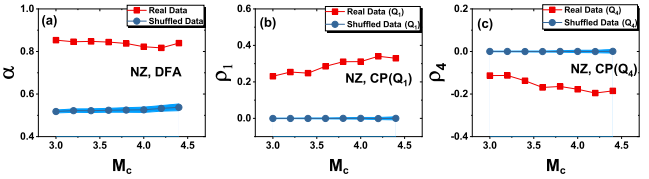


FIG. 6. Results on the New Zealand (NZ) earthquake catalog. (a) DFA memory scaling exponent $\alpha$ as a function of magnitude threshold $M_c$. (b, c) CP memory coefficient $\rho_1$ and $\rho_4$ as a function of magnitude threshold $M_c$. The blue lines in the bottom of each subplot indicate the DFA scaling exponent $\alpha$ and the CP memory measure $\rho_1$, $\rho_4$ for the control randomly shuffled records, averaged over 1000 realizations; the shaded region indicates the error bars (std).

robust, ∼0.75, i.e., the size of $dt$ does not affect the memory exponent. Thus, the return intervals, the number of events, and released energy are significantly correlated and have very similar scaling exponents. This apparent universal scaling exponent $\alpha$ can potentially be used to validate the performance of earthquake forecasting models and for narrowing the range of model parameters; we use it below to optimize the ETAS model parameters.

## III. CONDITIONAL PROBABILITY ANALYSIS FOR REAL SEISMIC CATALOGS

According to Omori's law [27], earthquake events tend to cluster in time due to the time-dependent relaxation of the crust through the release of triggered aftershocks. The rate $n(t)$ of aftershocks above a certain magnitude $M_c$ decays with time $t$ as $n(t) \sim t^{-p}$. This clustering and power-law decay indicates that both short- and long-range correlations (memories) exist in seismic data. To better characterize and understand all types of memory in earthquake events, we now further develop and apply a general conditional probability (CP) method; see also [18].

We begin by sorting the full time series of recurrence intervals in ascending order and divide it into four 25% quantiles, i.e., the first quantile $Q_1$ represents shortest 25% of waiting times, etc. We next consider the distribution of recurrence times $\tau$ that follow a prior recurrence time $\tau_0$, $P(\tau|\tau_0)$, where $\tau_0$ belongs to either one of the quantiles at the extremities, $Q_1$ or $Q_4$. Essentially, given that a prior recurrence time was either short (in $Q_1$) or long (in $Q_4$), we ask what is the distribution of the subsequent recurrence times. In records without memory, $P(\tau|\tau_0)$ should be independent of $\tau_0$ and should be identical to $P(\tau)$. Figures 5(a) and 5(c) show the pair distribution function (PDF) of waiting times ($Q$, $Q_1$, and $Q_4$) for the Israeli and Italian catalogs, respectively. The figure suggests,

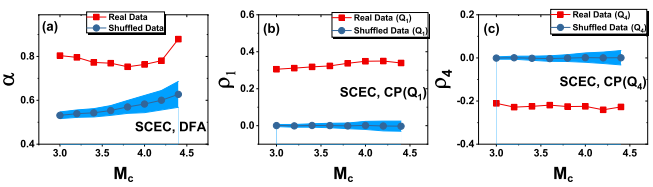


FIG. 7. The same as Fig. 6 for the Southern California Earthquake Center (SCEC) catalog.

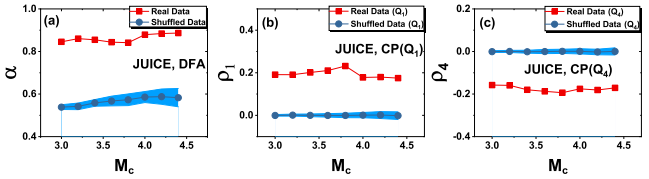


FIG. 8. The same as Fig. 6 for the Japan Unified High-Resolution Relocated Catalog for Earthquakes (JUICE).

as in Ref. [18], that $P(\tau|\tau_0)$ depends strongly on the previous recurrence time $\tau_0$ such that short recurrence times are more likely to be followed by short ones and long recurrence times follow long ones. Note that the present study is different from the analysis of Refs. [6,18], as the distribution of recurrence times in our analysis is not rescaled and normalized by the mean event rate. This is since (i) short interevent times are also considered, and (ii) the difference between $Q_1$ and $Q_4$ is much clearer compared with the rescaled case (Fig. 2 for Ref. [6]).

We next consider the cumulative distribution function (CDF) of the recurrence times and quantify the difference between the overall CDF of the unconditional recurrence times for the entire catalog $Q$ and the CDF for a given quantile by considering the area represented in the gap between the curves [see Figs. 5(b) and 5(d)]. Here, we denote the CDF of the recurrence time for $Q$, $Q_1$, and $Q_4$ as $CQ(\tau)$, $CQ_1(\tau)$, and $CQ_4(\tau)$, respectively. To this end, we define the level of memory for $Q_1$ as $\rho_1 = \int (CQ_1(\tau) - CQ(\tau))d\tau / \int d\tau$ and, similarly, the level of memory for $Q_4$ as $\rho_4 = \int (CQ_4(\tau) - CQ(\tau))d\tau / \int d\tau$. Thus, $0 \leqslant \rho_1 \leqslant 1$ and $-1 \leqslant \rho_4 \leqslant 0$, and higher $|\rho_1|$ (or $|\rho_4|$) implies stronger memory while $\rho_1 = 0$ (or $\rho_4 = 0$) implies no memory. Figure 5 shows the results for Israeli and Italian earthquake catalogs. We find $\rho_1 = 0.248$, $\rho_4 = -0.193$ for $Q_1$ and $Q_4$ of the Israeli catalog, whereas $\rho_1 = 0.260$, $\rho_4 = -0.153$ for $Q_1$ and $Q_4$ of the Italian catalog. Figures 2(c)–2(f) suggest that the values of $\rho$ are robust and do not depend on $M_c$. These results are consistent with the DFA results [Figs. 1, 2(a), and 2(b)]. To study the dependence of the correlations ($\alpha$, $\rho_1$, and $\rho_4$) on the geographical location (tectonic setting), we performed the DFA and CP analysis for other earthquake catalogs, including New Zealand (NZ), Southern California Earthquake Center (SCEC), Japan Unified High-Resolution Relocated Catalog for Earthquakes (JUICE), and the Preliminary Determination of Epicenters (PDE) global earthquake catalogs. The results are presented in Figs. 6–9. We find that for all catalogs and for all studied magnitudes the values of $\alpha$, $\rho_1$, and $\rho_4$ are quite robust. A detailed description of each catalog is given in the Appendix.

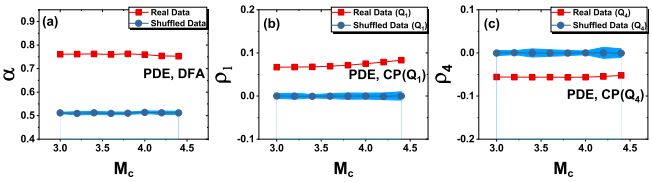


FIG. 9. The same as Fig. 6 for the Preliminary Determination of Epicenters (PDE) catalog.

## IV. MEMORY ANALYSIS IN THE ETAS MODEL

### A. ETAS model

We will now study the possible origin of the memory in real data by analyzing the ETAS model [28], which can also be used to generate synthetic earthquake catalogs. ETAS is a stochastic point-process model in which background events occur through a Poisson process in time with rate $\mu$, and all past events above a threshold magnitude $M_c$ may produce aftershocks. It has been successfully used for operational earthquake forecasting, e.g., the complex Amatrice-Norcia seismic sequence [29]. The ETAS model is based on two well-established empirical basic laws: (i) the Gutenberg-Richter law [30], $\log N = a - bm$, where $N$ is the number of events in a given time period with magnitude $\geqslant m$ and $a$, $b$ are constants; (ii) the Omori law, $n(t) = K/(c+t)^p$, where $n(t)$ is the number of aftershocks after time $t$ and $K$, $c$, $p$ are constants. The conditional intensity function $\lambda$ in the ETAS model is

$$\lambda(t|H_t) = \mu + A \sum_{i:t_i<t} \exp[\alpha_M(m_i - M_z)]\left(1 + \frac{t - t_i}{c}\right)^{-p}, \tag{1}$$

where $t_i$ are the times of the past events and $m_i$ are their magnitudes; $H_t = \{(t_i, m_i); t_i < t\}$ is the history of occurrence. $\lambda(t|H_t)$ provides the probability to have an earthquake above a threshold magnitude $M_z$ at time $t$, given the earthquake history. Here, $A = K/c^p$ is the occurrence rate of earthquakes in the Omori law at zero lag [11], and $\alpha_M$ is called the productivity parameter.

### B. Effects of background rate $\mu$

We next investigate how the background rate $\mu$ affects the memory in the ETAS model. We have only considered variations of $\mu$ without changing the branching ratio (see below) by setting $A = 6.26$, $c = 0.007$, $\alpha_M = 1.4$, and $p = 1.13$. (These are the prior estimates for the Italian catalog, and $\mu = 0.2$ [31].) Figure 10 shows that the memory coefficients $\alpha$ (of the DFA) and $\rho$ (of the CP for $Q_1$ and $Q_4$) decay with $\mu$, which suggests, as expected, that $\mu$ significantly affects the memory such that smaller $\mu$ implies stronger memory. This is because the variation in $\mu$ arises from the effect of the interference of temporally overlapping aftershock subsequences or "correlated interevent times" [11]. As $\mu$ is increased, fewer aftershocks occur and more overlapping aftershock sequences take place, increasing the fraction of independent interevent times. Thus, the memory is destroyed. We also notice (not shown) that decreasing $\mu$ affects the distribution of recurrence times, changing it from a unimodal to a bimodal distribution [11].

### C. Effects of branching ratio $n'$

To further understand the origin of memory in the ETAS model, we also analyzed the effects on memory of the productivity parameter $\alpha_M$ and Omori's power law exponent $p$. Here we chose $\mu = 0.2$ (following the prior estimates

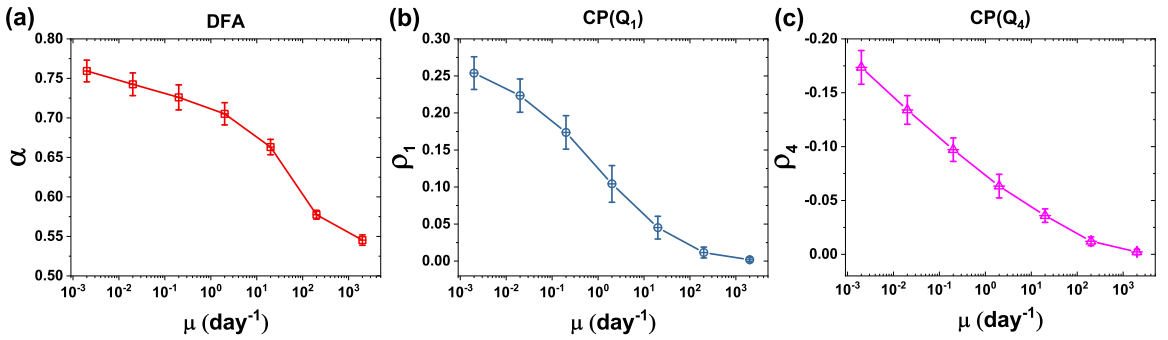


FIG. 10. Memory measures $\alpha$, $\rho_1$, and $\rho_4$ as a function of ETAS parameter $\mu$. (a) DFA scaling exponent $\alpha$, (b) CP coefficient $\rho_1$ for short recurrence times $Q_1$, and (c) CP coefficient $\rho_4$ for long recurrence times $Q_4$. The other ETAS parameters used are $A = 6.26$, $\alpha_M = 1.4$, $p = 1.13$, $c = 0.007$, and $M_c = 3.0$ for the Italian catalog, following [31]. The error bars (std) are based on 100 independent simulation realizations.

for the Italian catalog [31]), where the other ETAS model parameters are the same as mentioned above. Figure 11 presents simulation results of the model for $p \in [1.1, 2.0]$ and $\alpha_M \in [0.1, 1.5]$. We find that the memory in the ETAS model strongly depends on both $p$ and $\alpha_M$: smaller $p$ and larger $\alpha_M$ imply stronger memory. Note that memory patterns for DFA ($\alpha$) and CP ($\rho_1$, $\rho_4$) are highly consistent. This result can be explained by the branching ratio $n'$, the average number of aftershocks generated by each parent event. As the branching ratio grows, correlated aftershocks increase and the background fraction decreases, resulting in stronger memory. The branching ratio $n'$ is obtained by integrating $A\exp(\alpha_M m)(1+\frac{t}{c})^{-p}$ over both time and magnitude from 0 to $\infty$ and is given by [32]: $n' = \frac{Ac}{p-1}\frac{\beta}{\beta-\alpha_M}$, where $\beta = b\ln(10)$, is obtained from the Gutenberg-Richter law; here we chose $b = 1.0$. When writing Eq. (1) as $\lambda(t|H_t) = \mu + A\sum_{i:t<t_i}\exp[\alpha_M(m_i - M_z)]\frac{p-1}{c}(1+\frac{t-t_i}{c})^{-p}$, then $n' = \frac{A(p-1)}{c}\frac{\beta}{\beta-\alpha_M}$ is also related with $c$ and $p$. The condition (with $p > 1$ and $\beta > \alpha_M$) for physical stability is that $n'$ is finite and less than 1 [33]. The parameter $\mu$ has no effect on aftershock generation. We find that $n'$ is proportional to $\alpha_M$ and $1/p$, which agrees well with our results (see Fig. 11). To determine the sample uncertainty, we performed 100 independent simulation realizations for each combination of parameter values. The error bars (standard deviations) are shown in Fig. 12. We also present the DFA of the occurrence times for a specific simulation realization with ETAS parameters, $\mu = 0.2$, $A = 6.26$, $\alpha_M = 1.5$, $p = 1.1$, and $c = 0.007$, see Fig. 13. The model results yield the same $\alpha$ as in real data. The CP analysis for the same realization is shown in Fig. 14. Figure 15 demonstrates that the values of $\alpha$, $\rho_1$, and $\rho_4$ are robust, do not depend on $M_c$ in the ETAS model, and are similar to the results based on the real catalogs.

However, Figs. 10 and 11 show that the ETAS model can reproduce the same memory as in real catalogs, only for a small range of parameter values, i.e., $\mu = 0.2$, $\alpha_M = 1.5$, and $p = 1.1$. These are close to, though still statistically different from, the previous parameters found, which were $\mu = 0.2$, $A = 6.26$, $\alpha_M = 1.4$, $p = 1.13$, and $c = 0.007$ [31]. In estimating the ETAS model parameters for an earthquake catalog, the ETAS parameters are commonly inverted from the data based on the point-process maximum likelihood (ML) method, by the Davidon-Fletcher-Powell algorithm [28], or by simulated annealing [31]. Our results provide a narrow range of values that are capable of reproducing the memory and provide an intuition for why only these values are reasonable. Thus, our results and methods can be used to improve the choice of parameters of the ETAS model, which can potentially help to improve the forecasting rate of earthquakes.

## V. EARTHQUAKE FORECASTING

Clearly, earthquake forecasting is a very important challenge due to the devastating possible outcome of earthquakes. The forecasting accuracy depends on the temporal extension

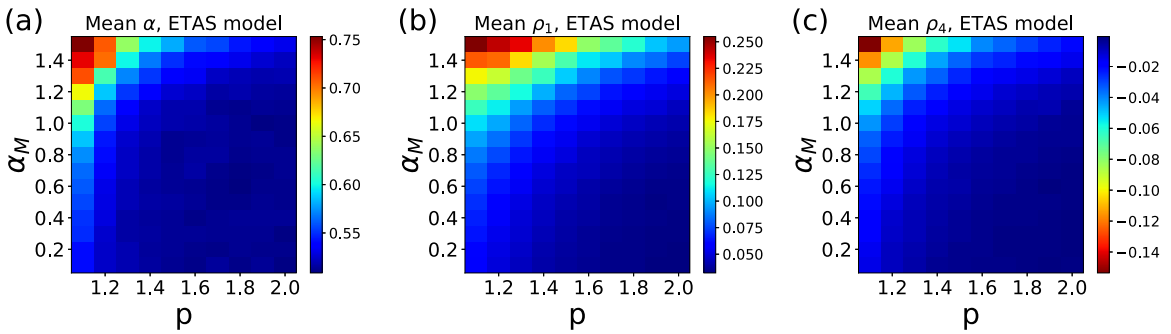


FIG. 11. The mean values of the (a) DFA scaling exponent $\alpha$, (b) CP coefficient $\rho_1$ for short recurrence times $Q_1$, and (c) CP coefficient $\rho_4$ for long recurrence times $Q_4$ as a function of ETAS model parameters, $p$ and $\alpha_M$. The other ETAS parameters used are $A = 6.26$, $\mu = 0.2$, and $c = 0.007$ for the Italian catalog, following [31].

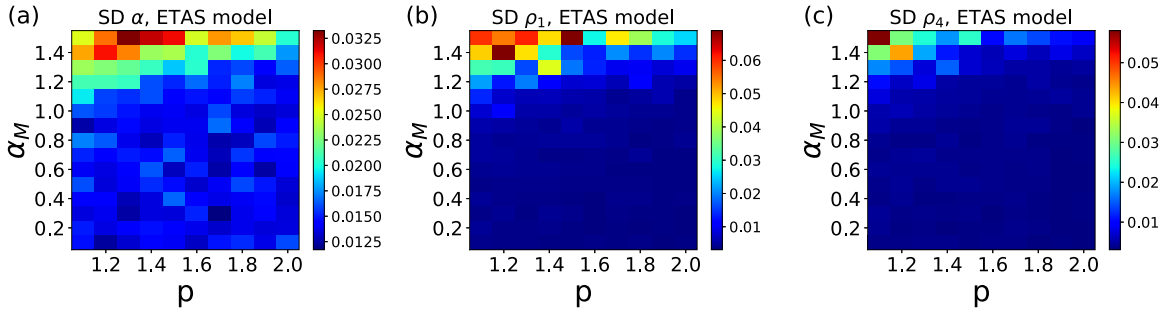


FIG. 12. The standard deviation (SD) of (a) DFA scaling exponent $\alpha$, (b) CP coefficient $\rho_1$ for short recurrence times $Q_1$, and (c) CP coefficient $\rho_4$ for long recurrence times $Q_4$. The other ETAS parameters used are $A = 6.26$, $\mu = 0.2$, and $c = 0.007$.

$T$ of the period we are focusing on—e.g., for long-term forecasting, $T$ is an interval of decades and centuries; for intermediate-term forecasting, $T$ is of the order of months; and for short-term forecasting, $T$ is within the interval of a few seconds to weeks [34]. The above ranges can be related to the ratio between a typical time scale, such as the average intertime between large shocks $\langle \Delta T \rangle$ and $T$. Below we show, based on the real Italian earthquake catalog, that the ETAS model (when considering the memory effects) can significantly increase short-term forecasting.

As a test case we forecast the cumulative number of events, NC, after the Capitignano 5.7 main shock that happened on 18 January 2017 [35] by using the ETAS model. The cumulative number of earthquakes at time $t$ is given by integrating Eq. (1) from 0 to $t$ [36]. We define the forecasting rate as

$$f(t) = \frac{|NC_f(t) - NC_r(t)|}{NC_r(t)}, \tag{2}$$

where $NC_f(t)$ is the forecasting cumulative number of earthquakes and $NC_r(t)$ is the real cumulative number. Here, $0 \leqslant f(t) \leqslant 1$, and smaller $f(t)$ implies higher forecasting accuracy.

Our forecasting results are presented in Fig. 16(a) for 14 days (two weeks) after the Capitignano 5.7 main shock. We can also see here that the ETAS model, when considering the memory, improves the forecasting rate [37]. Figure 16(b) depicts the forecasting rate $f(t)$ [Eq. (2)] within 14 days after the main shock and indicates that our choice of ETAS model parameters improves the forecasting by more than 20% (maximum). Thus, it is seen that the ETAS model parameters that are based on the correlation results discussed above can significantly improve the forecasting power of earthquakes. Here we chose $M_c = 2.9$, since the earthquake events with $M \geqslant 2.9$ after 2017 for the Italian catalog are complete. The choice of the parameters in the forecasting algorithm are based on the DFA ($\alpha$) and CP ($\rho_1$, $\rho_4$) scaling parameters.

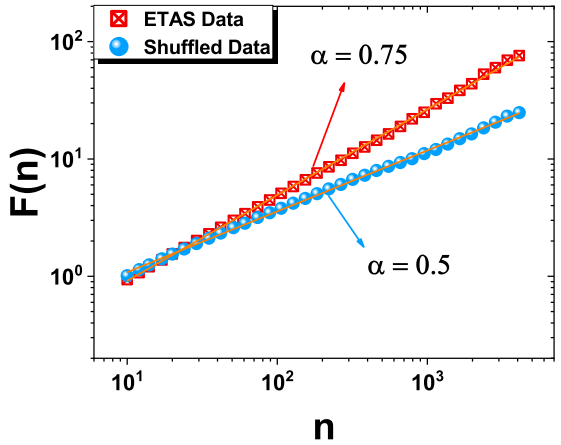


FIG. 13. DFA of the interoccurrence times from the ETAS model, with parameters $A = 6.26$, $\mu = 0.2$, $p = 1.1$, $\alpha_M = 1.5$, and $c = 0.007$. The solid line is the best fitting line with slope $\alpha = 0.75$, R-squared $> 0.99$. For comparison, the shuffled data with slope $\alpha = 0.5$, indicating no memory, is presented.

## VI. SUMMARY

In summary, we have studied several seismic catalogs (recurrence times, number of events, and released energy) and found long-range memory for different magnitude thresholds $M_c$. We use the DFA and CP methods to quantify the level of memory and long-term correlations. We study the origin of the memory in real data by using synthetic catalogs generated by the ETAS model and find that the origin of memory in the ETAS model is influenced by: (i) the background (noise) rate parameter $\mu$, which affects the memory through interference of temporally overlapping aftershock subsequences, i.e., smaller $\mu$ leads to stronger memory, and (ii) the exponent relating the production of aftershocks as a function of magnitude, $\alpha_M$, and the power $p$ of Omori's law can also affect memory through the branching ratio of the ETAS model, i.e., smaller $p$ and larger $\alpha_M$ result in stronger memory. The information on the memory can be further incorporated into the algorithm to estimate the maximum likelihood parameters of the ETAS model and thus improve the forecast rate. We suggest

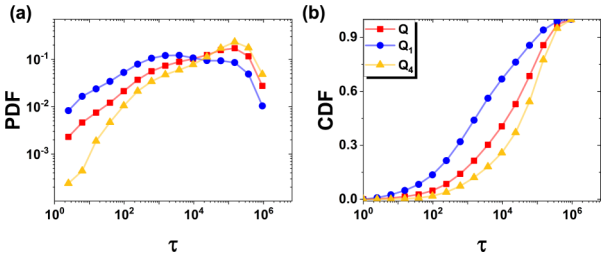


FIG. 14. Conditional (a) PDF and (b) CDF of the recurrence times $\tau$ for the ETAS model, with parameters $A = 6.26$, $\mu = 0.2$, $p = 1.1$, $\alpha_M = 1.5$, and $c = 0.007$.

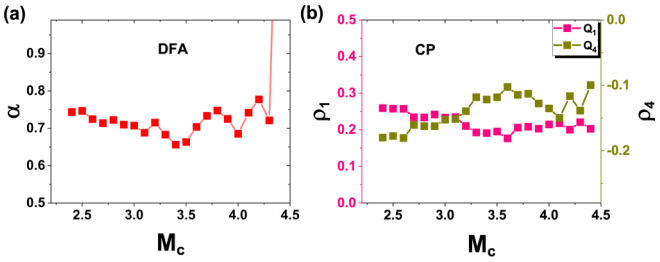


FIG. 15. (a) DFA memory scaling exponent $\alpha$ as a function of magnitude threshold $M_c$; (b) CP memory coefficients $\rho_1$ and $\rho_4$ as a function of magnitude threshold $M_c$ for ETAS model, with parameters $A = 6.26$, $\mu = 0.2$, $p = 1.1$, $\alpha_M = 1.5$, and $c = 0.007$.

that the approach developed here has the potential to improve earthquake forecasting capability when fitting it to earthquake clustering models, such as the ETAS model, with spatial components [38] and short-term earthquake probability models [39].

## ACKNOWLEDGMENTS

This work was partially supported by Italy-Israel project OPERA, which is funded jointly by the Italian Ministry of Foreign Affairs and International Cooperation and the Israeli Ministry of Science, Technology, and Space (MOST). We also thank the Israel Science Foundation, ONR, Japan Science Foundation, BSF-NSF, ARO, the EU 2020 project RISE (Project No. 821115), and DTRA (Grant No. HDTRA-1-10-1-0014) for financial support. J.F. thanks the East Africa Peru India Climate Capacities–EPICC project, which is part of the International Climate Initiative (IKI).

## APPENDIX: DATA DESCRIPTION

The Italian earthquake catalog contains earthquake events in the Italy region. Most events are contained within the region 35°N–48°N and 6°E–20°E. In the present study, we chose the time period from 1-1-1981 until 25-4-2017. The magnitude threshold is 3.0, and the number of events is 8554. See Ref. [40] for the source of data.

The Israeli earthquake catalog contains earthquake events in the Israeli region. Most events are contained within the region 27°N–35°N and 31°E–38°E. In present study, we chose the time period from 1-1-1986 until 3-10-2017. The magnitude threshold is 2.0, and the number of events is 9789. Again, see Ref. [40] for the source of data.

The New Zealand (NZ) earthquake catalog contains earthquake events in the New Zealand region. Most events are contained within the region 35°S–50°S and 160°E–185°E. In the present study, we chose the time period from 1-1-1988 until 31-10-2018. The magnitude threshold is 3.0, and the number of events is 103,234. See Ref. [41] for the source of data.

The Southern California Earthquake Center (SCEC) earthquake catalog contains earthquake events in the Southern California region. Most events are contained within the region 32°N–37°N and 238°E–246°E. In the present study, we chose the time period from 1-1-1988 until 31-10-2018. The magnitude threshold is 3.0, and the number of events is 9569. See Ref. [42] for the source of data.

The Japan Unified High-Resolution Relocated Catalog for Earthquakes (JUICE) contains earthquake events in Japan. Most events are contained within the region 30°N–46°N and 128.6°E–146°E. The time period is from 1-10-2000 until 31-12-2012. The magnitude threshold is 3.0, and the number of events is 13,708. See Ref. [43] for the source of data.

The Preliminary Determination of Epicenters (PDE) catalog contains worldwide earthquake events. In the present study, we chose the time period from 1-1-1983 until 31-7-2013. The magnitude threshold is 3.0, and the number of events is 297,996. See Ref. [44] for the data source.

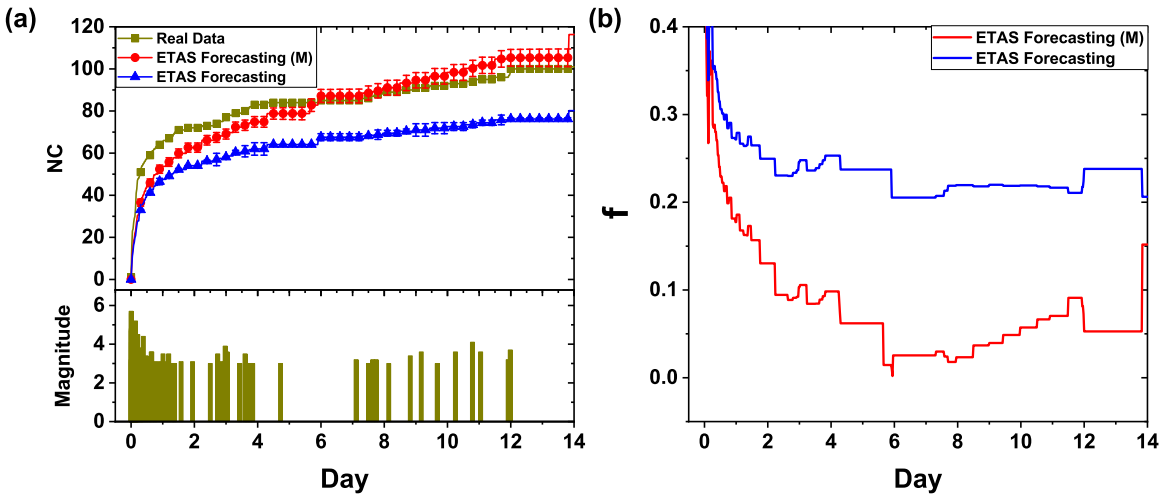


FIG. 16. The cumulative number of earthquakes for real Italian catalog and for ETAS model forecasting. (a) Short-term 14-day forecasting; (b) forecasting rates vs time in the ETAS model when considering memory (top, red) compared to the common regular forecasting [31] (bottom, blue). The red line, "ETAS forecasting (M)," depicts the results when using our choice of parameters that are based on the memory results; the blue line shows the results based on previous choice of parameters. A plot of event magnitude vs time in real Italian catalog is shown in the bottom-left panel.

[1] D. Sornette, Phys. Rep. **313**, 237 (1999).

[2] D. Sornette, *Critical Phenomena In Natural Sciences—Chaos, Fractals, Selforganization and Disorder: Concepts and Tools*, Springer Series in Synergetics (Springer-Verlag, Berlin/Heidelberg, 2006).

[3] P. Bak, K. Christensen, L. Danon, and T. Scanlon, Phys. Rev. Lett. **88**, 178501 (2002).

[4] C. G. Sammis and D. Sornette, Proc. Natl. Acad. Sci. **99**, 2501 (2002).

[5] D. L. Turcotte, *Fractals and Chaos in Geology and Geophysics* (Cambridge University Press, Cambridge, 1997).

[6] A. Corral, Phys. Rev. Lett. **92**, 108501 (2004).

[7] J. Davidsen, S. Stanchits, and G. Dresen, Phys. Rev. Lett. **98**, 125502 (2007).

[8] T. Mäkinen, A. Miksic, M. Ovaska, and M. J. Alava, Phys. Rev. Lett. **115**, 055501 (2015).

[9] G. Molchan and T. Kronrod, Geophys. J. Int. **162**, 899 (2005).

[10] A. Saichev and D. Sornette, Phys. Rev. Lett. **97**, 078501 (2006).

[11] S. Touati, M. Naylor, and I. G. Main, Phys. Rev. Lett. **102**, 168501 (2009).

[12] H. V. Ribeiro, L. S. Costa, L. G. A. Alves, P. A. Santoro, S. Picoli, E. K. Lenzi, and R. S. Mendes, Phys. Rev. Lett. **115**, 025503 (2015).

[13] B. B. Mandelbrot and J. R. Wallis, Water Resour. Res. **5**, 967 (1969).

[14] E. Koscielny-Bunde, A. Bunde, S. Havlin, and Y. Goldreich, Physica A (Amsterdam, Neth.) **231**, 393 (1996).

[15] E. Koscielny-Bunde, A. Bunde, S. Havlin, H. E. Roman, Y. Goldreich, and H.-J. Schellnhuber, Phys. Rev. Lett. **81**, 729 (1998).

[16] C.-K. Peng, J. Mietus, J. M. Hausdorff, S. Havlin, H. E. Stanley, and A. L. Goldberger, Phys. Rev. Lett. **70**, 1343 (1993).

[17] A. Bunde, S. Havlin, J. W. Kantelhardt, T. Penzel, J.-H. Peter, and K. Voigt, Phys. Rev. Lett. **85**, 3736 (2000).

[18] V. N. Livina, S. Havlin, and A. Bunde, Phys. Rev. Lett. **95**, 208501 (2005).

[19] S. Lennartz, V. N. Livina, A. Bunde, and S. Havlin, Europhys. Lett. **81**, 69001 (2008).

[20] C.-K. Peng, S. V. Buldyrev, S. Havlin, M. Simons, H. E. Stanley, and A. L. Goldberger, Phys. Rev. E **49**, 1685 (1994).

[21] S. V. Buldyrev, A. L. Goldberger, S. Havlin, R. N. Mantegna, M. E. Matsa, C.-K. Peng, M. Simons, and H. E. Stanley, Phys. Rev. E **51**, 5084 (1995).

[22] Y. Ashkenazy, M. Lewkowicz, J. Levitan, H. Moelgaard, P. E. B. Thomsen, and K. Saermark, Fractals **06**, 197 (1998).

[23] P. Gasperini, B. Lolli, and G. Vannucci, Bull. Seismol. Soc. Am. **103**, 2227 (2013).

[24] The completeness catalogs can be downloaded from: https://www.dropbox.com/home/OPERA_SharedFolder/CATALOGS.

[25] J. F. Eichner, J. W. Kantelhardt, A. Bunde, and S. Havlin, Phys. Rev. E **73**, 016130 (2006).

[26] J. N. Tenenbaum, S. Havlin, and H. E. Stanley, Phys. Rev. E **86**, 046107 (2012).

[27] F. Omori, Journal of the College of Science **7**, 111 (1894).

[28] Y. Ogata, J. Am. Stat. Assoc. **83**, 9 (1988).

[29] W. Marzocchi, M. Taroni, and G. Falcone, Sci. Adv. **3**, e1701239 (2017).

[30] B. Gutenberg and C. F. Richter, Bull. Seismol. Soc. Am. **34**, 185 (1944).

[31] A. M. Lombardi, Sci. Rep. **5**, 8417 (2015).

[32] D. Sornette and M. J. Werner, J. Geophys. Res.: Solid Earth **110**, B09303 (2005).

[33] D. Sornette and A. Helmstetter, Phys. Rev. Lett. **89**, 158501 (2002).

[34] L. de Arcangelis, C. Godano, J. R. Grasso, and E. Lippiello, Phys. Rep. **628**, 1 (2016).

[35] E. Falcucci, S. Gori, C. Bignami, G. Pietrantonio, D. Melini, M. Moro, M. Saroli, and F. Galadini, Tectonics **37**, 2425 (2018).

[36] Y. Ogata, Tectonophysics **169**, 159 (1989).

[37] We used the SASeis2006 program package for forecasting the future earthquake events. The package can be downloaded from https://www.ism.ac.jp/~ogata/Ssg/softwares.html.

[38] Y. Ogata, Ann. Inst. Stat. Math. **50**, 379 (1998).

[39] M. C. Gerstenberger, S. Wiemer, L. M. Jones, and P. A. Reasenberg, Nature (London) **435**, 328 (2005).

[40] https://www.dropbox.com/home/OPERA_SharedFolder

[41] https://quakesearch.geonet.org.nz

[42] http://service.scedc.caltech.edu

[43] http://www.hinet.bosai.go.jp/topics/JUICE/?LANG=en

[44] https://www.usgs.gov